Metal-Containing Carbon Clusters: Structures, Isomerization, and Formation of NbC_n^+ Clusters

David E. Clemmer and Martin F. Jarrold*

Contribution from the Department of Chemistry, Northwestern University, 2145 Sheridan Road, Evanston, Illinois 60208

Received May 22, 1995[⊗]

Abstract: Injected ion drift tube techniques, including ion mobility measurements and annealing and fragmentation studies, have been used to examine the isomers present for NbC_n^+ (n = 15−50) clusters. Isomers attributed to niobium-containing monocyclic and bicyclic rings, graphitic sheets, and metallofullerenes have been identified. Monocyclic rings, where the niobium atom appears to be either inserted into or bound to the outside of the ring, dominate for NbC_n^+ with n < 22. Isomers assigned to bicyclic rings are first observed and become dominant around NbC_{22}^+. Unlike the bicyclic rings for C_n^+ and LaC_n^+, the NbC_n^+ bicyclic rings do not anneal into monocyclic rings. They probably consist of two rings joined together by a niobium atom. An isomer attributed to NbC_n^+ graphitic sheets is present for n > 22 and becomes important for clusters with around 30 carbon atoms. Metallofullerenes are first observed for NbC_{28}^+ and become a major isomer for clusters with n > 31. Both endohedral metallofullerenes and networked metallofullerenes (where the metal atom is part of the cage) have been identified. For clusters with more than around 30 carbon atoms the NbC_n^+ bicyclic rings can be annealed into metallofullerenes and, for the smaller ones, metal-containing graphitic sheets. The isomers observed for NbC_n^+ are similar to those found for pure C_n^+ and LaC_n^+, but the niobium atom has a substantial effect on the properties and the abundances of the different isomers.

Introduction

Since the discovery of fullerenes[1] and techniques to generate macroscopic quantities of some fullerenes,[2,3] a substantial effort has been devoted to doping carbon clusters with metal atoms.[4] The structures and properties of endohedral metallofullerenes[4,5,6] (formed by laser and arc vaporization of metal−carbon composites) and exohedral metallofullerenes[7,8] (formed by attaching metal atoms to C_{60}) have been studied in some detail. Metallocarbohedranes (M_8C_{12}),[9,10] another class of metal-containing carbon cluster, have also received considerable attention recently, although these species have not yet been produced in macroscopic quantities. Clearly the stoichiometric variability and the many possible interesting geometries of composite metal−carbon clusters make them a fascinating class of atomic cluster. Moreover, the production of several metallofullerenes in bulk quantities suggests that there is a high probability for creating novel and perhaps useful materials from metal−carbon clusters.

The strategy we have adopted to probe these metal−carbon clusters is to first examine how the incorporation of a single metal atom affects the geometries and properties, compared to those for the pure carbon cluster analogues, before extending these studies to clusters containing more than one metal atom. We have recently reported studies of LaC_n^+ clusters.[11,12,13] For both pure C_n^+ clusters[14,15] and LaC_n^+ clusters, fullerenes and several non-fullerene isomers (including monocyclic rings, bicyclic rings, and graphitic fragments) have been identified. As discussed in detail below, NbC_n^+ clusters show similar structural isomers. But there are also important differences,[16] and so these studies provide a chance to understand how variations in the properties of the metal atom affect the isomers that form, and allow important insight into the nature of metal−carbon bonding.

The experimental studies described here were performed using injected ion drift tube techniques. Information about the geometries of the cluster ions and the isomer distributions was obtained from ion mobility measurements. The mobility of a gas-phase ion depends on its collision cross section which in turn depends on the geometry, so structural isomers can be separated on the basis of their different mobilities. While first demonstrated for organic ions in the 1970s,[17] this approach has

[⊗] Abstract published in *Advance ACS Abstracts*, August 15, 1995.

(1) Kroto, H.; Heath, J. R.; O'Brien, S. C.; Curl, R. F.; Smalley, R. E. *Nature* **1985**, *318*, 162.

(2) Kratschmer, W.; Lamb, L. D.; Fostiropolos, K.; Huffman, D. R. *Nature* **1990**, *347*, 354.

(3) Kratschmer, W.; Fostiropolos, K.; Huffman, D. R. *Chem. Phys. Lett.* **1990**, *170*, 167.

(4))For a recent review see: Bethune, D. S.; Johnson, R. D.; Salem, J. R.; deVries M. S.; Yannoni, C. S. *Nature* **1993**, *366*, 123.

(5) Weiss, F. D.; O'Brien, S. C.; Elkind, J. L.; Curl, R. F.; Smalley, R. E. *J. Am. Chem. Soc.* **1988**, *110*, 4464.

(6) Chai, T.; Guo, T.; Jin, C.; Haufler, R. E.; Chibante, L. P. F.; Fure, J.; Wang, L.; Alford J. M.; Smalley, R. E. *J. Phys. Chem.* **1991**, *95*, 7564.

(7) Roth, L. M.; Huang, Y.; Schwedler, J. T.; Cassady, C. J.; Ben-Amotz, D.; Kahr, B.; Freiser, B. S. *J. Am. Chem. Soc.* **1991**, *113*, 6298.

(8) McElvany, S. W. *J. Phys. Chem.* **1992**, *96*, 4935.

(9) Wei, S.; Guo, B. C.; Purnell, J.; Buzza, S.; Castleman, A. W. *Science* **1992**, *255*, 818. Guo, B. C.; Kerns, K. P.; Castleman, A. W. *Science* **1992**, *255*, 1411. Wei, S.; Guo, B. C.; Purnell, J.; Buzza, S.; Castleman, A. W. *J. Phys. Chem.* **1992**, *96*, 4166. Guo, B. C.; Wei, S.; Purnell, J.; Buzza, S.; Castleman, A. W. *Science* **1992**, *256*, 515. Guo, B. C.; Kerns, K. P.; Castleman, A. W. *J. Am. Chem. Soc.* **1993**, *115*, 7415.

(10) Pilgrim, J. S.; Duncan, M. A. *J. Am. Chem. Soc.* **1993**, *115*, 4395. Pilgrim, J. S.; Duncan, M. A. *J. Am. Chem. Soc.* **1993**, *115*, 6958. Pilgrim, J. S.; Brock, L. R.; Duncan, M. A. *J. Phys. Chem.* **1995**, *99*, 544.

(11) Clemmer, D. E.; Shelimov, K. B.; Jarrold, M. F. *Nature* **1994**, *367*, 718.

(12) Clemmer, D. E.; Shelimov, K. B.; Jarrold, M. F. *J. Am. Chem. Soc.* **1994**, *116*, 5971.

(13) Shelimov, K. B.; Clemmer, D. E.; Jarrold, M. F. *J. Phys. Chem.* **1994**, *19*, 12819.

(14) von Helden, G.; Hsu, M.-T.; Gotts, N; Bowers, M. T. *J. Phys. Chem.* **1993**, *97*, 8192.

(15) Hunter, J. M.; Fye, J. L.; Jarrold, M. F. *J. Chem. Phys.* **1993**, *99*, 1785.

(16) Clemmer, D. E.; Hunter, J. M.; Shelimov, K. B.; Jarrold, M. F. *Nature* **1994**, *17*, 248.

0002-7863/95/1517-8841$09.00/0

only recently been applied to atomic clusters.[18] Comparison of measured mobilities to those estimated for assumed geometries is used to attribute the observed features to specific geometries.[19] Information on the annealing and fragmentation of the cluster ions is obtained by increasing their injection energy, so that they undergo a rapid transient heating cycle as they enter the drift tube. As the injection energy is increased the clusters may be heated to the point where they isomerize, or even dissociate.[19,20] The isomer distribution is followed by ion mobility measurements to determine which isomers isomerize or fragment. Isomer resolved annealing experiments have previously been reported for Si_n^+,[19,21] Ge_n^+,[22] Al_n^+,[23] C_n^+,[15,24,25,26] and LaC_n^+ [13] clusters.

Experimental Section

Our injected ion drift tube apparatus has been described in detail previously[27] so only a brief description is given here. NbC_n^+ clusters were produced by pulsed laser vaporization of a niobium−carbon composite rod in a continuous flow of helium. Previous unsuccessful attempts at producing NbC_n^+ clusters have been interpreted as indicating that NbC_n^+ metallofullerenes are not stable.[28] Only small quantities of NbC_n^+ clusters were generated when Nb:C ratios of 1:60 and 1:30 were used. However, with an Nb:C ratio of 1:10, NbC_n^+ clusters form readily. To enhance the cluster ion signal, a 1.1 kV electron beam was injected into the buffer gas flow ~1 cm before the exit aperture. The niobium−carbon composite rods were made by two methods. In the first,[29] NbC (Johnson Matthey, 99%) was mixed with graphite cement (Dylon, Grade GC) and the mixture was slurried into a teflon-coated mold. The NbC-cement slurry was cured at ~130 °C for 4 h and then the sample rod was removed from the mold and heated in a tube furnace under a helium atmosphere at ~1000 °C for ~8 h in order to remove volatile impurities from the cement. In the second method, NbC and carbon (Johnson Matthey 99.9995%) powders were hydraulically pressed into a mold in order to form a cementless rod. The mass spectra and drift time distributions measured for rods generated by the two methods were not significantly different.

After exiting the source the NbC_n^+ cluster ions were focused into a quadrupole mass spectrometer where a specific cluster was mass selected. Mass selection of a pure beam of NbC_n^+ clusters presented some difficulties because of the presence of hydrogenated contaminants, $NbC_nH_x^+$, and C_{n+8}^+ ions which lie only 3 amu above the NbC_n^+ ions. To avoid these contaminants many of the experiments reported here were performed with the resolving power of the first quadrupole set sufficiently high that nearly isotopically pure $Nb^{12}C_n^+$ clusters were selected and contaminants comprise less than a few percent of the cluster beam.

After mass selection the cluster ions were focused into a low-energy ion beam and injected at various energies into the drift tube which contains ~5.0 Torr of helium buffer gas at room temperature. The buffer gas pressure inside the drift tube is measured using a capacitance manometer. The drift tube is 7.62 cm long with 0.025 cm diameter entrance and exit apertures and the body is made of three electrically insulated guard rings to ensure a uniform electric field close to the drift axis. The drift field was 13.12 V cm^{-1}. After travelling across the drift tube, the small fraction of ions that exit are focused into a second quadrupole mass spectrometer. This quadrupole can be scanned in order to determine what products are formed (in dissociation or reactivity studies) or used to transmit only the ion of interest (for drift time measurements). After exiting the second quadrupole, ions are detected by an off-axis collision dynode and dual microchannel plates.

Drift time distributions were measured by injecting 50-μs pulses of cluster ions into the drift tube and recording the arrival time distribution at the detector with a multichannel scaler using 10-μs resolution. These measurements are performed both with and without the buffer gas in the drift tube, and the time that the clusters spend traveling across the drift tube is determined from the difference between these two measurements (plus some small corrections to account for the fact that the kinetic energy of the ions exiting the drift tube depends on whether the buffer gas is present). The reduced mobility is then determined from[30]

$$K_o = \frac{L}{t_D E} \frac{P}{760} \frac{273.2}{T} \quad (1)$$

where t_D is the average drift time, E is the electric field, L is the length of the drift tube, and P is the pressure in Torr. The reproducibility of the mobility measurements is excellent, different measurements usually agree to within 1%. The absolute accuracy of these measurements is a few percent. It is mainly limited by end effects (for example, the buffer gas flow near the entrance and exit apertures of the drift tube, and the penetration of the injected ions which reduces the effective length of the drift tube). The variation of the measured mobilities as a function of injection energy provides some information about the penetration of the injected ions. These variations are approximately the same size as the precision of the mobility measurements. Thus penetration effects are small, a result which is consistent with the predictions of simple hard sphere collision models of the injection process.[31]

Results

Drift Time Distributions at an Injection Energy of 150 eV. Figure 1 shows typical drift time distributions measured for NbC_{18}^+−NbC_{32}^+ with an injection energy of 150 eV. At this injection energy the clusters are significantly heated by collisions with the He buffer gas as they enter the drift tube, so a considerable amount of annealing (isomerization) occurs and a small fraction (less than 5%) of the injected ions dissociate. Thus, the distributions shown in Figure 1 are due to relatively stable isomers. Odd-numbered clusters with fewer than 22 carbon atoms (NbC_n^+ with n = 15, 17, 19, and 21) show two peaks in the drift time distributions while the peak occurring at shorter times is only a small shoulder for even-numbered clusters in this size range. The isomer arriving at longer times dominates the distributions for NbC_{18}^+−NbC_{21}^+. Starting at NbC_{22}^+, the peak at shorter time (~630 μs) begins to dominate the distribution for both odd and even numbered clusters. This peak correlates with the middle peak in the drift time distributions for NbC_{25}^+ and NbC_{27}^+ and to the slowest peaks for NbC_{30}^+ and larger clusters. The shoulder near ~630 μs for NbC_{23}^+ is the first evidence of an isomer that becomes prominent by NbC_{27}^+ and dominates the distributions for NbC_{29}^+ and NbC_{31}^+. A peak corresponding to the most compact isomer that we observe, the metallofullerene, first appears for NbC_{28}^+ at ~550 μs and becomes a major isomer for n > 31.

(17) Tou, J. C.; Boggs, G. U. *Anal. Chem.* **1976**, *48*, 1351. Carr, T. W. *J. Chromatogr.* **1977**, *15*, 85. Hagen, D. F. *Anal. Chem.* **1979**, *51*, 870. Karpas, Z.; Cohen, M. J.; Stimac, R. M.; Wernlund, R. F. *Int J. Mass Spectrom. Ion Proc.* **1986**, *83*, 163. For a recent review of ion mobility spectrometry see: St. Louis, R. H.; Hill, H. H. *Crit. Rev. Anal. Chem.* **1990**, *21*, 321.

(18) von Helden, G.; Hsu, M.-T.; Kemper, P. R.; Bowers, M. T. *J. Chem. Phys.* **1991**, *95*, 3835.

(19) Jarrold, M. F.; Constant, V. A. *Phys. Rev. Lett.* **1992**, *67*, 2994.

(20) Jarrold, M. F.; Honea, E. C. *J. Phys. Chem.* **1991**, *95*, 9181.

(21) Jarrold, M. F.; Bower, J. E. *J. Chem. Phys.* **1992**, *96*, 9180.

(22) Hunter, J. M.; Fye, J. L.; Jarrold, M. F.; Bower, J. E. *Phys. Rev. Lett.* **1994**, *73*, 2063.

(23) Jarrold, M. F.; Bower, J. E. *J. Chem. Phys.* **1993**, *98*, 2399.

(24) Hunter, J.; Fye, J. L.; Jarrold, M. F. *Science*, **1993**, *260*, 784; *J. Phys. Chem.* **1993**, *97*, 3460.

(25) von Helden, G.; Gotts, N. G.; Bowers, M. T. *Nature* **1993**, *363*, 60.

(26) Shelimov, K. B.; Hunter, J. M.; Jarrold, M. F. *Int. J. Mass Spectrom. Ion Proc.* **1994**, *138*, 17.

(27) Jarrold, M. F.; Bower, J. E.; Creegan, K. M. *J. Chem. Phys.* **1989**, *90*, 3615.

(28) Guo, T.; Smalley, R. E.; Scuseria, G. E.; *J. Chem. Phys.* **1993**, *99*, 352.

(29) Chai, Y.; Guo, T.; Jin, C.; Haufler, R. E.; Chibante, L. P F.; Fure, J.; Wang, L.; Alford, J. M.; Smalley, R. E. *J. Phys. Chem.* **1991**, *95*, 7564.

(30) Mason, E. A.; McDaniel, E. W. *Transport Properties of Ions in Gases*; Wiley: New York, 1988.

(31) Jarrold, M. F.; Clemmer, D. E. unpublished.

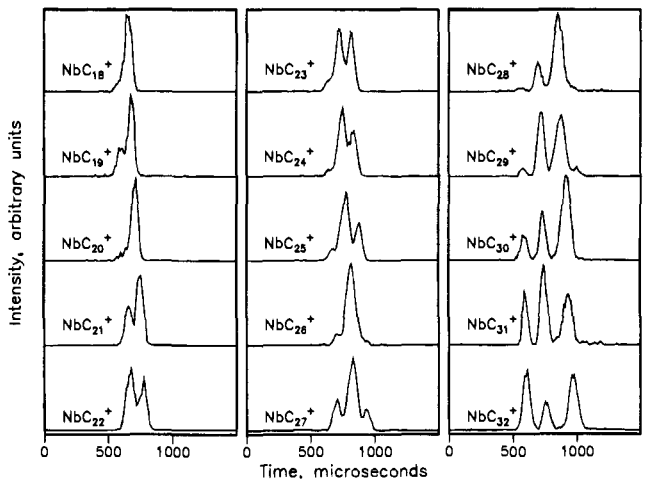

Figure 1. Drift time distributions for NbC_n^+ (n = 18–32). The distributions were recorded with an injection energy of 150 eV and have been scaled to a buffer gas pressure of 5.000 Torr.

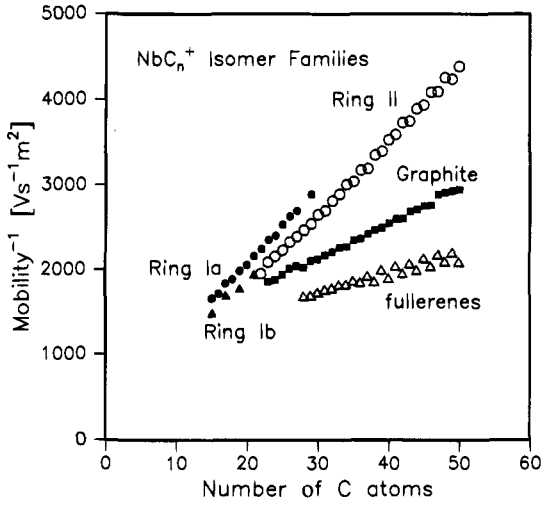

Figure 2. Plot of the inverse mobility against cluster size for the NbC_n^+ isomers observed in the drift time distributions.

Figure 2 shows the inverse reduced mobilities determined for all of the peaks in the drift time distributions for NbC_{15}^+–NbC_{50}^+ clusters at an injection energy of 150 eV. It is clear that the peaks shown in Figure 2 fall into several distinct families of isomers. We have labeled these families *Ring Ia* (observed for NbC_{15}^+–NbC_{27}^+), *Ring Ib* (observed for NbC_{15}^+, NbC_{17}^+, NbC_{19}^+, and NbC_{21}^+), *Ring II* (observed for NbC_{22}^+–NbC_{50}^+), *Graphite* (observed for NbC_{23}^+–NbC_{50}^+), and *Fullerene* (observed for NbC_{28}^+–NbC_{50}^+). C_n^+ clusters[14] and LaC_n^+ clusters[12] show similar isomers, and the labels used here were derived by comparing the present data to those published previously for pure C_n^+ and LaC_n^+ clusters. The assignment of plausible geometries to the observed isomers will be discussed in detail below. In brief, the assignments are the following: *Ring Ia* and *Ring Ib* are attributed to monocyclic carbon rings with the metal atom in different locations; the *Ring II* isomers are assigned to bicyclic rings (generated by fusing two monocyclic rings); the features labeled *Graphite* are attributed to roughly-planar metal-containing graphitic fragments; and the features labeled *Fullerene* are assigned to networked and endohedral fullerenes.

Some of the NbC_n^+ families of isomers show odd/even alternations in their mobilities. The most dramatic example of this behavior is observed for the NbC_n^+ *Fullerene* family. NbC_{2n}^+ fullerenes containing at least 38 carbon atoms have significantly smaller inverse mobilities than their NbC_{2n-1}^+ counterparts, even though the latter species contain one fewer carbon atom. The *Ring II* family also shows small odd/even alternations in their mobilities. In addition, the *Ring Ib* isomers are prominent only for the odd-numbered clusters NbC_{15}^+, NbC_{17}^+, NbC_{19}^+, and NbC_{21}^+.

Information about whether a given peak in the drift time distribution results from more than one isomer can be obtained by comparing the measured peak shapes to those calculated from the transport equation for ions in the drift tube,[30]

$$\Phi(t) = \int dt_P P(t_P) \frac{C}{(Dt)^{1/2}} (v_D + L/t)\left[1 - \exp\left(\frac{-r_0^2}{4Dt}\right)\right] \exp\left(\frac{-(L - v_D t)^2}{4Dt}\right) \quad (2)$$

In this equation, $\Phi(t)$ is the flux of ions passing through the exit aperture as a function of time, r_o is the radius of the entrance aperture, v_D is the measured drift velocity, C is a constant, $P(t_p)\,dt_p$ is the distribution function for the pulse of ions entering the drift tube, and D is the diffusion constant, which under low-field conditions is related to the measured mobility by the expression $D = Kk_BT/e$ (where k_B is the Boltzmann constant and e is the electronic charge). When the drift time distribution calculated using this expression is in good agreement with the measured distribution it *suggests* that only a single isomer is present. When the measured drift time distribution is significantly broader than the calculated distribution it indicates that there are at least two structural isomers present with slightly different mobilities. For the *Ring Ia*, *Graphite*, and *Fullerene* isomers (except for NbC_{38}^+) the calculated drift time distributions are in excellent agreement with the measured ones. The drift time distribution for NbC_{38}^+ *Fullerene* is slightly broader than the calculated distribution. The measured drift time distributions for the *Ring II* isomers are also slightly broader than the calculated ones, indicating that at least two types of *Ring II* isomer are present with slightly different mobilities. The drift time distributions for the *Ring II* isomer of pure C_n^+ clusters are also slightly broader than the calculated ones.

Figure 3 shows the relative abundances of the isomers discussed above plotted against cluster size. These results were obtained with an injection energy of 150 eV. Uncertainties in the relative isomer populations are 5–10%. The *Ring I* isomers dominate for the smaller clusters. The *Ring II* isomer first appears around NbC_{22}^+ and then dominates the isomer distribution for clusters with up to around 30 carbon atoms. The isomers labeled *Graphite* first appear at about the same cluster size as *Ring II*, and become a major isomer for clusters with around 30 carbon atoms. The fullerene becomes the dominant isomer for NbC_n^+ clusters with odd $n > 31$ and even $n > 40$.

Annealing NbC_{25}^+. Figure 4 shows drift time distributions for NbC_{25}^+ collected at injection energies of 50 and 150 eV. The two largest peaks in these distributions fall into the *Ring II* (~750 μs) and *Ring I* (~860 μs) families of isomers. There is no significant difference in the relative abundance of the two major peaks at these injection energies, and no difference is observed with injection energies up to 250 eV. Drift time distributions collected for NbC_{24}^+ also show no significant injection energy dependence over this range. At the higher injection energies a significant amount of fragmentation occurs. NbC_n^+ (n = 24 and 25) dissociate primarily by loss of neutral C_3, and to a lesser degree C_5. C_3 loss dominates the dissociation pattern for the analogous C_n^+ isomers.[26] For NbC_n^+ (n = 24 and 25) a series of peaks, corresponding to loss of neutral NbC_x (x = 2–7) fragments, are also observed. Loss of neutral

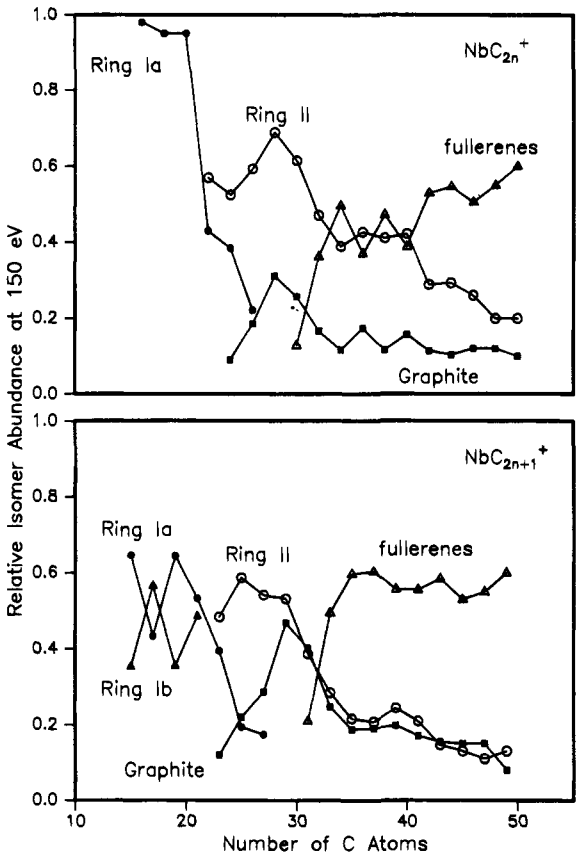

Figure 3. Plot of the relative abundances of the observed isomers against cluster size. The results shown in the figure are for an injection energy of 150 eV. The upper plot shows results for clusters with an even number of carbon atoms, and the lower plot is for the odd-numbered clusters.

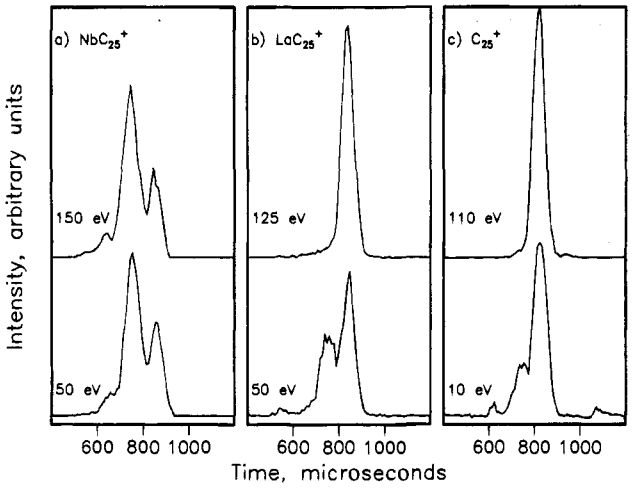

Figure 4. Drift time distributions measured for (a) NbC_{25}^+ at injection energies of 50 and 150 eV, (b) C_{25}^+ at 10 and 110 eV, and (c) LaC_{25}^+ at injection energies of 50 and 150 eV.

niobium-containing fragments suggests that the ionization energies of small NbC_x and C_{n-x} clusters are similar. Drift time distributions recorded for LaC_{25}^+ and C_{25}^+ over a similar range of injection energies are also shown in Figure 4. For both LaC_{25}^+ and C_{25}^+ clusters two peaks (which also fall into *Ring I* and *Ring II* families) are observed at low injection energies while only one (the *Ring I* isomer) is observed for both systems at the higher injection energies. Annealing studies of NbC_n^+ (n = 25, 26, 35, 36, 39, and 40) clusters show that, in general, the fraction of *Ring I* isomer is not enhanced at high injection

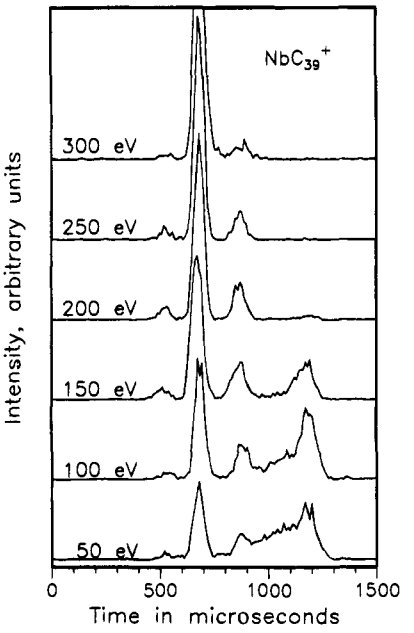

Figure 5. Drift time distributions for NbC_{39}^+ collected over a range of injection energies, from 50 to 300 eV.

energies, a result that is fundamentally different from our results for lanthanum-doped[32] and pure carbon[26] clusters of the same size.

Annealing NbC_{39}^+. Figure 5 shows drift time distributions measured for NbC_{39}^+ at injection energies ranging from 50 to 300 eV. We have also obtained detailed annealing data for NbC_{35}^+, NbC_{36}^+, and NbC_{40}^+. The data for these clusters are similar to the data shown here for NbC_{39}^+. At 50 eV, a narrow peak at ~680 μs and a broader distribution from ~800 to 1300 μs is observed. The narrow peak falls into the *Fullerene* family. The broad distribution shows some definite structure which becomes clearer as the injection energy is raised. At an injection energy of 100 eV, the portion of the broad distribution between ~900 and ~1150 μs decreases and three peaks (the metallo-fullerene, and peaks centered near ~870 and ~1180 μs) are observed. At 150 eV, only these three peaks, which fall into the *Fullerene* (~680 μs), *Graphite* (~870 μs), and *Ring II* (~1180 μs) families, remain. The *Other* isomers observed at 50 eV, with drift times from ~900 to ~1150 μs, must be more compact than the *Ring II* species but less compact than the *Graphite* and *Fullerene* isomers. Analogous isomers for the pure carbon clusters have been attributed to tricyclic and tetracyclic rings.[14] Above 150 eV, the *Ring II* isomer essentially disappears and the distributions are dominated by the *Graphite* and *Fullerene* isomers. As mentioned above the detailed annealing data for NbC_{35}^+, NbC_{36}^+, and NbC_{40}^+ are similar to those described here for NbC_{39}^+. One notable difference is that there is not a significant increase in the relative abundance of *Graphite* for NbC_{39}^+ or NbC_{40}^+ as the injection energy is raised to 150 eV, while a significant increase in the abundance of this isomer is observed for the smaller clusters (NbC_{35}^+ and NbC_{36}^+).

Figure 6 shows the relative abundances of the various isomers for NbC_{39}^+ and the fraction that dissociates plotted against injection energy. The isomers labeled *Other* have drift times between 900 and 1150 μs. At low injection energies the isomer distribution consists of roughly equal fractions of *Ring II*, *Fullerene*, and *Other* isomers. At 100 eV no dissociation is observed, but at higher injection energies the fraction of NbC_{39}^+

(32) Shelimov, K. B.; Clemmer, D. E.; Jarrold, M. F. *J. Phys. Chem.* **1995**, *99*, 11376.

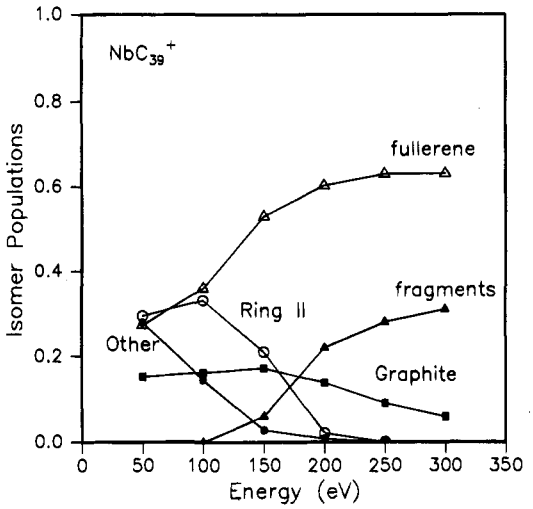

Figure 6. Plot of the isomer populations (determined from the drift time distributions) for NbC_{39}^+ at injection energies of 50−300 eV.

that dissociates increases gradually to a maximum of ~30% at the highest injection energy studied, 300 eV. The primary fragment ion results from loss of C_3. At the higher injection energies (250 and 300 eV), product ions resulting from the loss of NbC_n (n = 2−7) fragments were also observed, but they comprise less than 10% of the products. At an injection energy of 100 eV the relative abundance of the *Other* isomers decreases while the *Ring II* and *Fullerene* populations increase. Since no dissociation is observed at 100 eV, the *Other* isomers presumably convert into the *Ring II* and *Fullerene* isomers. Similar behavior has been observed for pure C_n^+ clusters. At 150 eV the relative abundances of the *Other* isomers continues to decrease, and the relative abundance of the *Ring II* isomers also decreases substantially. Since there is little fragmentation at 150 eV, it appears most of the *Other* and *Ring II* isomers convert into fullerenes. Above 150 eV more of the *Ring II* isomer appears to anneal into *Fullerene*. At the higher injection energies the relative abundance of *Graphite* starts to decrease, probably because it dissociates.

Estimates of Activation Energies. An estimate of the activation energies associated with the annealing and fragmentation processes can be deduced from the injection energy thresholds. To accomplish this it is necessary to determine the degree of collisional excitation that occurs as the ions enter the drift tube, and account for the statistical nature of the annealing or fragmentation process. The fraction of the clusters' kinetic energy that is transferred into internal energy as the clusters enter the drift tube is assumed to be given by a modified impulsive collision model:[20]

$$F_{ie} = C\frac{1}{N}\sum\frac{1 - m_i/M}{1 + m_i/m} \qquad (3)$$

where C is an empirical correction factor, N is the number of atoms in the cluster, m_i is the mass of atom number i in the cluster, M is the total mass of the cluster, m is the mass of a buffer gas atom, and the summation goes over all the atoms forming the cluster. The isomerization rate of a vibrationally excited cluster is estimated using RRK theory.[33] The reaction time is assumed to be of the order of the time between collisions with the buffer gas. Because of the difficulty in estimating the degree of collisional excitation that occurs, we do not expect the values obtained in this way to be accurate to more than ~1.0 eV. However, the relative values are expected to be more reliable, and so the activation energies for NbC_n^+ can be compared with those for C_n^+ and LaC_n^+ clusters. Estimates of the activation energies for the annealing of several NbC_n^+ clusters are given in Table 1. The *Ring II* isomers of the odd-numbered NbC_n^+ clusters, NbC_{35}^+ and NbC_{39}^+, begin annealing into fullerenes at injection energies that are ~50 eV lower than for the even numbered analogues, NbC_{36}^+ and NbC_{40}^+. So the estimated activation energies are substantially smaller for the odd-numbered NbC_n^+ clusters than for the even-numbered ones (see Table 1). Note that while the activation energies for the odd- and even-numbered clusters are significantly different, the efficiencies of fullerene formation, for the clusters studied, are quite similar. Similar odd−even variations in the activation energies were *not* observed for the LaC_n^+ clusters that have been studied.

(33) Steinfeld, J. I.; Fransisco, J. S.; Hase, W. L. *Chemical Kinetics and Dynamics*; Prentice-Hall: Englewood Cliffs, NJ, 1989.

Table 1. Estimated Activation Energies for the Annealing of NbC_n^+, LaC_n^+, and C_n^+ Rings[a]

size (n)	NbC_n^+	C_n^+	LaC_n^+
24	NC[b]		
25	NC[b]	2.4[c]	2.2[c]
26		2.4[c]	2.2[c]
35	2.7[d]		3.1[d]
36	3.3[d]		3.1[d]
39	2.5[d]		
40	3.0[d]	2.8[e]	2.8[d]

[a] Estimates for the NbC_n^+ clusters are from this work. Unless otherwise stated, all other estimates are taken from ref 32. [b] No Conversion. Annealing of one isomer into another did not occur over the injection energy range studied. [c] Estimated activation energy for conversion of bicyclic rings into monocyclic rings. [d] Estimated activation energy for conversion of bicyclic rings into fullerenes. [e] Value taken from ref 15.

Discussion

Structural Assignments. (a) General Shapes. The general shapes of the NbC_n^+ isomers observed in these studies can be, to a large extent, deduced by comparison with the results and assignments given for the pure C_n^+ clusters[14] and LaC_n^+ clusters.[12] For pure C_n^+ clusters, monocyclic rings dominate the drift time distributions for C_{11}^+−C_{20}^+. Thus, it seems likely that the families of isomers that we observe for the smallest clusters studied here are due to NbC_n^+ incorporated into monocyclic carbon rings. Two families of monocyclic ring isomers have been observed for small LaC_n^+ clusters,[12] thus we have labeled the isomers observed for the small NbC_n^+ clusters as *Ring Ia* and *Ring Ib* in Figure 2. For pure C_n^+ clusters another family of isomers, beginning at C_{21}^+ and with inverse mobilities that parallel those for monocyclic rings, has been assigned to planar bicyclic ring isomers.[14] The NbC_n^+ data show an analogous family, beginning at NbC_{22}^+. These isomers have mobilities which are close to those for the carbon bicyclic rings and parallel the mobilities of the NbC_n^+ monocyclic rings. Thus, we have labeled this series as *Ring II* in Figure 2.

The pure C_n^+ clusters also show a family of isomers that is analogous to the NbC_n^+ family we have labeled *Graphite*. This family was first ascribed to a family of three-dimensional ring isomers by von Helden *et al.*[14] However, more recently Shelimov *et al.* have measured mobilities for this isomer over a more extended size range and the modeling of these data suggests that this feature is probably due to roughly planar graphitic fragments.[26] Addition of a transition metal to this system reopens the question of structure because metals can conceivably coordinate multiple rings, providing geometries that are not possible in the pure carbon clusters. Therefore, we will

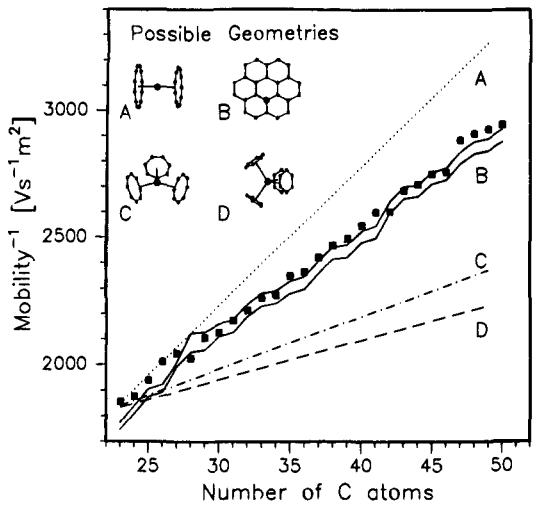

Figure 7. Inverse mobilities calculated for plausible geometries for the isomers labeled *Graphite*. The points are the measured inverse mobilities. For *Structures A*, *C*, and *D* mobilities were calculated for NbC_{23}^+, NbC_{35}^+, and NbC_{45}^+ and a line drawn through the points. For *Structure B* (the graphitic sheet) calculations were performed for all cluster sizes. The geometries of the graphitic sheets were obtained by simply adding atoms to the outside of an existing sheet, and the small fluctuations in the calculated mobilities arise from the closing of hexagons.

consider graphitic sheet structures as well as metal bound ring systems as candidates for the family of isomers labeled *Graphite*.

The NbC_n^+ *fullerene* isomer is easily identified by comparison with the data for pure C_n^+ clusters. The odd/even alternations in the mobilities for this family are due to formation of endohedral and networked (where the metal atom is part of the cage) NbC_n^+ metallofullerenes. This assignment is consistent with the measured mobilities as well as chemical reactivity studies that have been discussed previously.[16] We will only briefly elaborate on the structural assignment of these species.

More detailed information about the nature of the NbC_n^+ isomers can be obtained by comparing the measured mobilities to mobilities calculated for model structures from momentum transfer theory[19] using the equation,

$$K_o = \frac{(18\pi)^{1/2}}{16}\left[\frac{1}{m_I}+\frac{1}{m_B}\right]^{1/2}\frac{e}{(K_BT)^{1/2}}\frac{1}{\sigma}\frac{1}{N} \qquad (4)$$

In this expression m_I and m_B are the masses of the ion and the buffer gas, respectively, N is the buffer gas number density, and σ is the collision cross section. The collision cross section is calculated by averaging over all possible orientations of the geometry in space assuming hard sphere interactions. For these calculations a He−C collision distance of 2.67 Å was used.[34] The Nb−He collision distance was taken to be 3.0 Å. Because there is only one niobium atom in each cluster the Nb−He collision distance can be varied substantially without significantly affecting the calculated mobilities.

(b) The *Graphite* Isomers. In addition to the graphitic fragment geometry suggested by comparison with the results of Shelimov *et al.*[26] for pure C_n^+ clusters, we have considered several other possible geometries for this family of isomers. These geometries are shown in Figure 7. In *Structure A* the niobium atom is sandwiched between two similarly sized carbon rings.[35] *Structure B* is a roughly-circular, niobium-containing graphitic sheet. In this structure we assume that the niobium atom replaces a carbon atom near the center but lies 1.4 Å above the plane. *Structure C* is a trigonal complex of three roughly equally sized rings surrounding a Nb atom,[36] and *Structure D* is a tetrahedral complex of four roughly equally sized rings surrounding a Nb atom.[36] For the model geometries described above we employed average C−C bond distances of 1.29 Å (for sp^1 carbons in the rings) and 1.42 Å (for sp^2 carbons in the graphitic fragments), and an Nb-C bond length of 2.0 Å.[37] Calculated inverse mobilities for these four, very different, geometries are shown in Figure 7. All four geometries give nearly identical mobilities for clusters with around 25 carbon atoms. However, only the mobilities calculated for *Structure B* (the graphitic fragment) are close to fitting the measured mobilities of these isomers over an extended cluster size range. So, assuming that there is not a systematic change in geometry with cluster size, we attribute these isomers to roughly planar graphitic fragments. Previous work has shown that this family of isomers is highly reactive with O_2 and N_2, a result that is also consistent with a graphitic fragment geometry.[16]

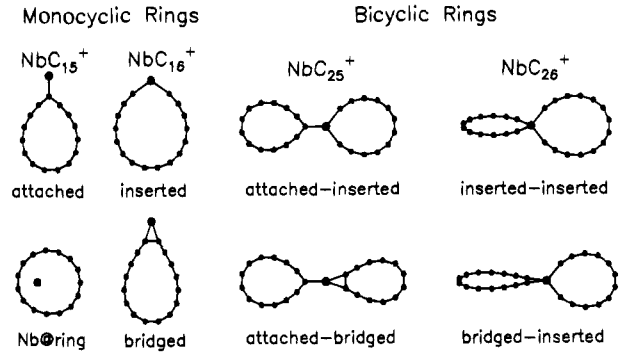

Figure 8. Some plausible ring geometries for NbC_n^+.

(c) The *Ring I* Isomers. A metal atom can attach to a monocyclic carbon ring in three basic geometries: it can be inserted into the ring, sit inside the ring, or bind to the outside of the ring (either bridged across a C−C bond or attached to a single carbon atom). These different geometries are shown schematically in Figure 8. Calculated inverse mobilities for the different geometries are shown plotted in Figure 9. The isomer with the metal atom inserted into the carbon ring has the largest calculated inverse mobility (short dashed line in Figure 9), but this is only slightly larger than the calculated inverse mobility for the isomer with the metal atom bound to the outside of the ring (short solid line in Figure 9). The calculated mobilities for the isomers with the metal atom bound outside the ring in the bridged and attached configurations are essentially identical. The dotted line extending over the entire size distribution in Figure 9 shows calculated inverse mobilities for monocyclic rings with the Nb sitting inside the ring. Comparison of the measured and calculated mobilities suggests that *Ring Ia* is probably a monocyclic ring with the Nb atom either inserted into the ring or bound to the outside, and the *Ring Ib* family is probably a monocyclic ring with the Nb atom sitting inside. The *Ring Ib* family of isomers is only observed over a narrow cluster size range: NbC_{15}^+, NbC_{17}^+, NbC_{19}^+, and possibly NbC_{21}^+. The *Ring Ib* isomers for LaC_n^+ are also much more abundant for clusters with an odd number of atoms, though for

(34) This value was deduced by fitting our data for the pure carbon monocyclic rings. Note that this He−C collision distance differs slightly from that used in some of our previous work because of an error in converting the calculated average collision cross sections into mobilities.

(35) A niobium-ring distance of 2.4 Å was used.

(36) A niobium-ring distance of 3.2 Å was used.

(37) Estimated from data taken from: Poole, A. D.; Williams, D. N.; Kenwright, A. M.; Gibson, V. C.; Clegg, W.; Hockless, D. C. R.; O'Neil, P. A. *Organometallics* **1993**, *12*, 2549. Huber, K. P.; Herzberg, G. *Constants of Diatomic Molecules*; Van Nostrand-Reinhold: New York, 1979.

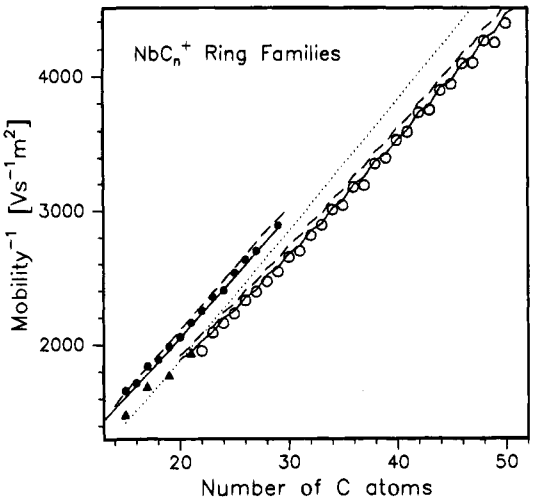

Figure 9. Comparison of the calculated inverse mobilities for the ring geometries with the experimental data for the *Ring Ia*, *Ring Ib*, and *Ring II* isomers. The short dashed line is a monocyclic ring with NbC_n^+ inserted into the ring, the short solid line is for a monocyclic ring with an Nb^+ either attached to or bridged on the outside of the ring, and the dotted line over the extended size regime is for a monocyclic ring with the Nb^+ near the center. The long dashed line shows the calculated mobilities for the *insertion-insertion* bicyclic ring isomer for NbC_{2n}^+ and the *attached-insertion* isomer for NbC_{2n-1}^+. The long solid line shows calculated mobilities for the *bridged-insertion* bicyclic ring isomer for NbC_{2n}^+ and the *attached-bridged* isomer for NbC_{2n-1}^+.

LaC_n^+ the *Ring Ib* isomers persist to larger cluster sizes. The inverse mobilities of the *Ring Ib* family of isomers are almost identical to those of the *Ring II* family that emerges for slightly larger clusters. The only real difference between these families is the strong odd/even oscillations in the abundances of the *Ring Ib* isomers which is not observed for the *Ring II* isomers. Thus we cannot completely rule out the possibility that the *Ring Ib* isomers and *Ring II* isomers are the same. The *Ring II* isomers are attributed to bicyclic rings. If the *Ring Ib* isomers were bicyclic rings they would be very highly strained.[26]

It is instructive to consider the chemical bonding in the NbC_n^+ *Ring I* isomers. For pure carbon monocyclic rings a cumulene (=C=C=C=C=) and polyacetylene (−C≡C−C≡C−) bonding scheme are believed to have similar energies, and the details of the chemical bonding in these rings are expected to vary with cluster size.[38] The first ionization energy of the Nb atom is significantly less than the ionization energy of small carbon clusters.[39,40] Thus it is reasonable to assume that the charge in the NbC_n^+ clusters is localized on the Nb. The second ionization energy of the Nb atom is quite large, so the Nb^+ will probably retain most of its valence electron density, enabling it to form up to four localized (essentially covalent) bonds with the carbon cluster. Thus for the isomer where the Nb^+ inserts into the carbon ring, the Nb^+ can be considered to simply substitute for a carbon atom.

Geometries where the Nb^+ is outside of the carbon ring (either in the attached or bridged configuration) formally require a divalent Nb^+ which drives the rest of the carbon ring to a polyacetylene bonding scheme. Because a polyacetylene bonding scheme can only propagate around a carbon ring with an even number of atoms, the attached configuration will probably be favored for an odd number of carbon atoms, and the bridged configuration favored for an even number. The isomer with the Nb^+ located inside the ring has the most favorable electrostatic interactions between Nb^+ and the ring. The apparent preference for an odd number of carbon atoms in the *Ring Ib* isomers may be related to larger electron affinities of odd-numbered carbon rings relative to the even-numbered ones.[41] This may promote more charge transfer from the Nb^+ ion to the odd-numbered rings and lead to additional electrostatic stabilization.[32] The most favorable electrostatic interactions will occur over a relatively narrow size range where the Nb^+ just fits inside the carbon ring; this may at least partly explain why *Ring Ib* isomers are only observed over a narrow size range.[32]

(d) The *Ring II* Isomers. The family of isomers that begins at NbC_{22}^+ has mobilities that are similar to those of pure C_n^+ bicyclic rings. However, there are small but significant odd−even variations in the mobilities of the NbC_n^+ *Ring II* isomers which are not observed for the pure C_n^+ bicyclic rings. The chemical reactivity of the *Ring II* isomers also shows oscillations: clusters with an even number of carbon atoms are essentially unreactive with O_2 and N_2, while at least some of the odd numbered *Ring II* isomers react readily.[16,42] Additional information can be obtained from the annealing studies performed for NbC_n^+, C_n^+, and LaC_n^+ clusters (see Figure 4). For pure carbon clusters, the bicyclic rings anneal into monocyclic rings when injected into the drift tube at 150 eV.[26] Bicyclic rings are more highly strained than monocyclic rings, and so the driving force for this isomerization process is strain relief.[26] LaC_n^+ bicyclic rings also open up to form monocyclic rings.[43] In contrast, the NbC_n^+ bicyclic rings appear to remain unchanged as the injection energy is raised. This observation provides an explanation for why the monocyclic rings are only observed for NbC_n^+ clusters containing fewer than 30 carbon atoms, but persist to significantly larger sizes for C_n^+ and LaC_n^+. Presumably for the larger C_n^+ and LaC_n^+ clusters, the monocyclic rings result from isomerization of bicyclic rings.

If the isomer distribution does not change when the injection energy is increased, this may indicate that the activation energy for isomerization is large, or that the activation energy is small so that the clusters leaving the source are already in an equilibrium distribution. The absence of monocyclic rings for the larger NbC_n^+ clusters suggests that the former explanation is the more likely, though it is also possible that the NbC_n^+ bicyclic rings are more stable than the C_n^+ and LaC_n^+ counterparts. A plausible interpretation of the differences between niobium-containing bicyclic rings and pure C_n^+ and LaC_n^+ bicyclic rings is that the niobium resides at the junction of the two rings and that Nb-C bonds fuse the rings together (this bonding scheme is less favorable for LaC_n^+ clusters with a formally divalent La^+). If this is the case, then the central location of the Nb atom between the rings could inhibit the ring-opening process.

Assuming that the Nb^+ provides the link between the two carbon rings in NbC_n^+ bicyclic rings, then the Nb^+ can bind to the rings by either inserting, bridging, or attaching (as described above for the monocyclic rings). Examples of plausible geometries for the bicyclic rings are shown in Figure 8. If the Nb^+ inserts into two carbon rings, by forming four single bonds, then we expect the rings to be orthogonal and the Nb^+ to have near tetrahedral coordination (as in the *inserted-inserted* geometry in Figure 8). This coordination is consistent with quantum

(38) See, for example: Feyereisen, M.; Gutowski, M.; Simons, J. *J. Chem. Phys.* **1992**, *96*, 2926.
(39) Weast, R. C., Ed. *CRC Handbook of Chemistry and Physics*, 63rd ed.; CRC Press: Boca Raton, FL 1982.
(40) Bach, S. B. H.; Eyler, J. R. *J. Chem. Phys.* **1990**, *92*, 358.
(41) Yang, S.; Taylor, K. J.; Craycraft, M. J.; Conceicao, J.; Pettiette, C. L.; Cheshnovsky, O.; Smalley, R. E. *Chem. Phys. Lett.* **1988**, *144*, 431.
(42) Clemmer, D. E.; Jarrold, M. F. Unpublished results.
(43) Shelimov, K. B.; Clemmer, D. E.; Jarrold, M. F. Unpublished results.

chemical calculations[44] which suggest $Nb(CH_3)_4^+$ (which also contains four single Nb^+-C single bonds) is tetrahedral. Formation of four Nb^+-C single bonds in this geometry fixes a polyacetylene bonding scheme in the rest of the carbon ring, which can only propagate for rings with an even number of carbon atoms. Thus the geometry where Nb^+ inserts into two carbon rings is expected to be favored for NbC_n^+ clusters with an even number of carbon atoms.

Another plausible geometry for the NbC_n^+ bicyclic rings has the Nb^+ inserted into one carbon ring and attached to another (*attached-inserted* in Figure 8). Quantum chemical calculations for $H_2C{=}Nb(CH_3)_2^+$ (which has an analogous Nb−C bonding scheme) show that this species is planar.[44] So we expect the *attached-inserted* bicyclic ring to be planar. Again the Nb^+ fixes a polyacetylene bonding scheme in the rings, which for the *attached* ring requires an odd number of carbon atoms. Thus, we expect the planar *attached-inserted* bicyclic ring to be favored for clusters with an odd number of carbon atoms.

Several other possible geometries can be conceived using the same ideas: the *attached-bridged* geometry shown in Figure 8 should be favored for NbC_n^+ clusters with an odd number of carbon atoms because the Nb^+ fixes a polyacetylene bonding scheme, and the *bridged-inserted* geometry, also shown in the figure, should be favored for even-numbered clusters. Along the same lines a *bridged-bridged* isomer and an *attached-attached* isomer (not shown in Figure 8) should also be favored for clusters with an even number of atoms.

Figure 9 compares the calculated inverse mobilities for the geometries discussed above with the mobilities measured for the *Ring II* isomers. The dashed line shows the calculated mobilities for the *inserted-inserted* NbC_{2n}^+ isomer and the *attached-inserted* NbC_{2n-1}^+ isomer. The solid line shows calculated mobilities for the *bridged-inserted* NbC_{2n}^+ isomer and the *attached-bridged* NbC_{2n-1}^+ isomer. The calculated inverse mobilities are in good agreement with the experimental values, and it is clear that the slightly different isomers that are expected to be present for clusters with an odd or even number of carbon atoms provide a way to explain the subtle odd/even oscillations in the measured mobilities. The good agreement between the mobilities calculated for the geometries discussed above and the measured mobilities cannot be regarded as proof that the clusters adopt these geometries because we cannot rule out the possibility that other geometries will also fit our experimental data. Furthermore, there remain some aspects of the mobility simulations, such as the consequences of charge localization and the effect of the long-range potential, which have not yet been fully explored.

The main difference between the various bicyclic ring isomers shown in Figure 8 is that those with an odd number of carbon atoms are planar, while most of the even-numbered ones are nonplanar with two orthogonal carbon rings. We believe that this difference may account for the low chemical reactivity of most of the even-numbered NbC_n^+ *Ring II* isomers.[16,42] With the two orthogonal carbon rings, and near tetrahedral coordination, the niobium atom is effectively shielded from chemical attack. On the other hand, in the planar geometries that are probably favored for clusters with an odd number of carbon atoms, the niobium is exposed and available for chemical reactions.

We noted above that the *Ring Ib* and *Ring II* isomers have similar mobilities (the only real difference being the large odd−even oscillations in the abundances of the *Ring Ib* isomers) and we could not dismiss the possibility that the *Ring Ib* isomers were bicyclic rings. So can we rule out the possibility that the *Ring II* isomers are really *Ring Ib* isomers (which are attributed to monocyclic rings with the metal inside the ring)? The dotted line in Figure 9 shows the mobilities calculated, over an extended size range, for a monocyclic ring with the metal atom inside. For small cluster sizes, this isomer and the various bicyclic ring isomers have similar calculated mobilities. However, with increasing cluster size, substantial differences emerge, and the calculated mobilities for the monocyclic ring isomer clearly do not fit the measured mobilities for the *Ring II* isomers. In addition, if the *Ring II* isomers were monocyclic rings, we can think of no compelling reason why some of the monocyclic ring isomers (*Ring Ia*) abruptly disappear for clusters with around 22 carbon atoms, while others persist up to at least 50 carbon atoms. Thus the arguments against the *Ring II* isomers being monocyclic rings appear to be strong.

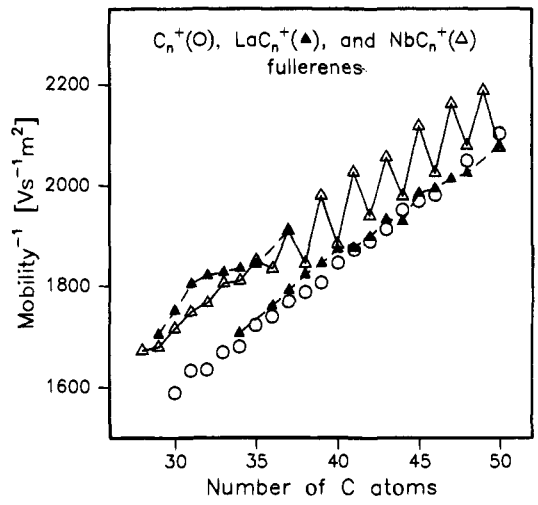

Figure 10. Inverse mobilities for the fullerene isomers plotted against the number of carbon atoms in the cluster for C_n^+ (open circles), LaC_n^+ (solid triangles), and NbC_n^+ (open triangles).

(e) The *Fullerene* Isomers. NbC_n^+ metallofullerenes are first observed for clusters containing 28 carbon atoms. Figure 10 shows the inverse reduced mobilities for NbC_n^+ fullerenes. Also shown are the results of similar measurements for pure C_n^+ fullerenes and LaC_n^+ metallofullerenes.[13] The C_n^+ and LaC_n^+ data are useful for establishing whether the metal is inside or outside of the carbon cage. LaC_{36}^+ and LaC_n^+ ($n > 37$) fullerenes have mobilities that are essentially identical to those measured for the C_n^+ analogues, indicating that they are endohedral metallofullerenes. LaC_{35}^+ and LaC_n^+ ($n < 34$) fullerenes have inverse mobilities that are substantially larger than the corresponding C_n^+ fullerenes. For these clusters, calculated inverse mobilities for model metallofullerene structures show that the lanthanum is either exohedral or networked (part of the carbon cage).[13] For LaC_{34}^+ and LaC_{37}^+ both endohedral and non-endohedral isomers have been identified. The result discussed above shows that the metal moves out of the fullerene cage for LaC_n^+ clusters with 34−37 atoms. The metal atom moves outside simply because the cage becomes too small to accommodate it. Lanthanum remains endohedral for smaller even-numbered clusters because the odd-numbered ones can easily form a networked metallofullerene (see below for a more detailed discussion of the networked geometry).

The measured mobilities for NbC_{37}^+ and smaller niobium metallofullerenes show similar behavior to the small LaC_n^+ fullerenes (the cage is too small to accommodate the metal atom). However, for the larger NbC_n^+ fullerenes only those with an even number of carbon atoms form endohedral

(44) These calculations were performed using the Gaussian-92 program. See: Frisch, M. J. *et al.*, Gaussian-92, Revision E.1; Gaussian, Inc.: Pittsburgh, PA, 1992.

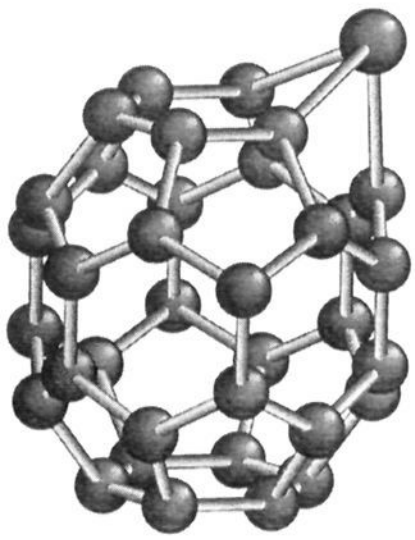

Figure 11. Schematic diagram of a networked metallofullerene geometry for NbC_{35}, obtained by replacing a carbon atom in C_{36} fullerene by a niobium atom.

metallofullerenes. The larger odd-numbered NbC_n^+ fullerenes have inverse mobilities that are substantially greater than their C_n^+ analogues, indicating that the metal atom is not encapsulated within the carbon cage. Closed cage fullerenes can only form with an even number of carbon atoms. Thus, for an odd number of carbon atoms there is a defect in the fullerene cage due to a missing carbon atom. The most reasonable explanation for our results for the NbC_n^+ fullerenes with an odd number of carbon atoms is that the metal substitutes for the missing carbon atom, stabilizing the resulting metallofullerene. A schematic diagram of such a networked metallofullerene structure is shown in Figure 11. Note that the metal protrudes above the surface of the fullerene cage because the metal−carbon bonds are significantly longer than the carbon−carbon bonds in the fullerene.

Mechanism of Cluster Growth. Information about the mechanism of NbC_n^+ cluster growth can be obtained by examining the isomer populations as a function of cluster size and from the annealing results. For pure carbon[14,25] it appears that medium-sized clusters grow by coalescence of rings, to give bicyclic, tricyclic, and even tetracyclic rings with increasing cluster size. It is relatively easy to open these rings up to relieve some of the strain.[26] Qualitatively similar behavior is observed for LaC_n^+ clusters.[32] The LaC_n^+ rings presumably form and isomerize in a similar manner to the pure carbon rings because the La^+, with only two valence electrons, is essentially a spectator. It can insert into, or bind to the outside of, a carbon ring, but once bound it has insufficient electron density to form strong bonds to other carbon atoms or to activate C−C bonds. On the other hand, Nb^+ (which has four valence electrons) can insert into, or bind to the outside of, a carbon ring and still have sufficient electron density to form additional bonds with other carbon atoms. Thus when a Nb-containing monocyclic ring encounters a carbon ring, a chemical interaction can occur through the niobium atom to yield a bicyclic ring where the niobium atom is at the junction between the two rings. The bicylic ring geometries shown in Figure 8 can be assembled from monocyclic ring precursors in this way. For example, the *attached-inserted* isomer can be made by attaching a pure carbon ring to the niobium in an NbC_n^+ monocyclic ring where the niobium is inserted into the ring.

When the C_n^+ clusters reach around 40 atoms, some of them convert into fullerenes when annealed (the balance dissociate to give small ring fragments). For the NbC_n^+ clusters studied here, and LaC_n^+ clusters, this process is much more efficient than for the pure C_n^+ clusters, and substantial amounts of fullerenes are formed for the metal-containing clusters with less than 40 carbon atoms. Networked and endohedral metallofullerenes are formed for the NbC_n^+ clusters, depending on whether there is an odd or even number of carbon atoms. The estimated activation energies for fullerene formation from the metal-containing carbon rings are similar to those for the pure carbon clusters. So the enhanced fullerene formation for the metal-containing clusters is not simply due to a decreased activation energy. We expect the reaction coordinate for transformation of the ring isomers to fullerenes to be complex, with several transition states, so that the effect of the metal may be to stabilize some of the critical intermediates. If this is the case then the activation energies that we estimate from these experiments should be viewed as effective activation energies rather than activation energies pertaining to a single maximum along the reaction coordinate. As can be seen from Table 1, the estimated activation energies for formation of networked NbC_n^+ fullerenes (for clusters with an odd number of carbon atoms) are systematically smaller than the activation energies for formation of endohedral NbC_n^+ fullerenes (for clusters with an even number of carbon atoms). The bicyclic rings are the main precursors for fullerene formation for NbC_n^+ in the size range examined here. The odd- and even-numbered bicylic rings have different chemical properties and slightly different mobilities, which we have attributed to different geometries. The different geometries of the odd- and even-numbered bicyclic rings may be responsible for the differing activation energies for fullerene formation.

Conversion of the rings into fullerenes is a remarkable structural transformation. This transformation is even more remarkable for the metal-containing carbon clusters, because it is also necessary to place the metal atom correctly—a feat which is accomplished with high efficiency for the NbC_n^+ clusters discussed here, and LaC_n^+ clusters. Several mechanisms have been proposed to account for the transformation of the ring isomers to fullerenes, including the "spiralling zipper" mechanism of Hunter *et al.*[24] and the "bud closing" mechanism of Schweigert *et al.*[45] The essential features of these mechanisms are first the preparation of a fullerene precursor and then the formation of a carbon network around the precursor, from the attached carbon chains. The driving force for this structural transformation is energy, sp^2 carbon atoms in the networks are substantially more stable than the sp^1 carbon atoms in the carbon rings. For the pure carbon clusters the threshold for fullerene formation occurs at around 40 atoms, and then the efficiency of fullerene formation increases slowly with cluster size. The low efficiency of fullerene formation for the smaller C_n^+ clusters has been attributed to the buildup of strain, either during the formation of the fullerene precursor or during the early stages of fullerene formation.[24] The metal atom may promote fullerene formation by relieving some of the strain. Graphitic sheets are also generated for metal-containing clusters with around 30 atoms, where the strain energy associated with generating the fullerene is large, and graphitic sheets are energetically competitive. The fact that both graphitic sheets and fullerenes are generated from the same precursors suggests that many different geometries are sampled during isomerization from the rings to the carbon networks (fullerenes and graphitic sheets).

Influence of the Metal Atom. Comparison of the results described above for NbC_n^+ clusters to results previously reported for pure C_n^+ clusters[14] and LaC_n^+ clusters[12] provides insight into how the nature of the metal atom influences the geometry of the carbon cluster. For LaC_n^+ clusters two families of monocyclic rings are present, one of which was attributed to a geometry with a divalent LaC_n^+ inserted into a carbon ring.[12,32] This isomer is only observed for LaC_n^+ clusters with an even

(45) Schweigert, V. A.; Alexandrov, A. L.; Morokov, Y. N.; Bedanov, V. M. *Chem. Phys. Lett.* **1995**, *235*, 221.

number of carbon atoms presumably because the divalent La^+ imposes a polyacetylene bonding scheme on the carbon ring. The analogous NbC_n^+ isomer with a tetravalent Nb^+ inserted into the ring appears to be present for both odd- and even-numbered clusters, though with NbC_n^+ other plausible ring geometries have similar calculated mobilities to the inserted isomer because the Nb−C bond length is relatively short.

The C_n^+ and LaC_n^+ bicyclic rings both anneal into monocyclic rings when injected into the drift tube at elevated kinetic energies. The NbC_n^+ bicyclic rings do not appear to anneal into monocyclic rings, and in addition the NbC_n^+ monocyclic ring isomers only persist up to relatively small cluster sizes (presumably because the monocyclic rings that are observed for the larger C_n^+ and LaC_n^+ clusters result from the annealing of bicyclic rings). The difference between the LaC_n^+ and NbC_n^+ clusters probably results because a lanthanum atom, inserted or attached to a carbon ring, has insufficient electron density remaining to form additional metal−carbon bonds, while a niobium atom can form additional metal-carbon bonds, leading to the variety of NbC_n^+ bicyclic ring isomers shown in Figure 8.

Insight into why niobium networks into large carbon cages, rather than being trapped inside (as observed for lanthanum), can be gained by considering the Nb^+ and La^+ ions.[16] Fullerenes with an odd number of carbon atoms have a defect site associated with a missing carbon atom. Nb^+ with four valence electrons should form strong chemical bonds with the sp^2 hybridized carbon atoms in the fullerene cage at the site of the missing carbon atom. On the other hand, the two valence electrons of La^+ cannot fully satisfy the four-electron defect in the cage and therefore cannot bond as strongly to the defect site. Also, because the second ionization energy of lanthanum is relatively low, charge transfer to the fullerene cage further reduces localized covalent interactions at the surface of the cage. Thus, the multiply charged lanthanum cation resides on the inside of the negatively charged fullerene cage in order to maximize electrostatic interactions. From these simple arguments it follows that networked MC_{2n-1}^+ metallofullerenes will most likely be formed from metals in group V (V, Nb, and Ta), and possibly also groups IV (Ti, Zr, and Hf) and VI (Cr, Mo, and W), of the periodic table, since the positive ions of these groups contain 4, 3, and 5 valence electrons, respectively. Furthermore, the first and second ionization energies of all of these metals are significantly higher than those for lanthanum and most of the other metals that are known to form endohedral metallofullerenes.[28] Networked metallofullerenes have recently been observed for some ZrC_n^+ clusters,[46] which further supports the ideas discussed above.

An important consequence of the presence of the metal atom is that it appears to enhance the abundances of the graphitic fragment and metallofullerene isomers. The graphitic fragment for pure C_n^+ clusters first appears at around C_{29}^+ and its abundance never amounts to more than a few percent.[14] For NbC_n^+ the graphitic fragment first appears at around NbC_{23}^+ and it becomes a major isomer for clusters with around 30 carbon atoms. The same is true for the metallofullerene, the fullerene isomer for pure C_n^+ emerges at around C_{30}^+, but it only becomes the dominant isomer for substantially larger clusters. For NbC_n^+ clusters the metallofullerene dominates almost as soon as it appears. Similar results have been obtained for LaC_n^+ clusters.[13] Several recent theoretical studies suggest that the graphitic fragments become more stable than the rings for C_n^+ clusters with less than 30 atoms.[47] So the low abundance of the graphitic sheets for C_n^+ clusters with around 30 atoms probably reflects the difficulty in making these species from the rings, presumably because of the buildup of strain during the isomerization process. For the metal-containing clusters, the metal presumably relieves some of the strain inhibiting their formation, and graphitic sheets are important isomers for NbC_n^+ clusters with around 30 atoms. For slightly larger clusters, where the fullerenes are not so highly strained, fullerenes form in preference to the graphitic sheets. For the C_n^+ clusters, fullerene formation only becomes significant for clusters with more than around 40 atoms, where the fullerenes are already preferred to the graphitic sheets. And so the graphitic sheets are not important isomers for the pure carbon clusters.

(46) Shelimov, K. B.; Jarrold, M. F. Unpublished results.

(47) Raghavachari, K.; Zhang, B.; Pople, J. A.; Johnson, B. G.; McGill, P. M. W. *Chem. Phys. Lett.* **1994**, *220*, 385. Taylor, P. R.; Bylaska, E.; Weare, J. H.; Kawai, R. *Chem. Phys. Lett.* **1995**, *235*, 558.

Summary

Mobility measurements for NbC_n^+ clusters (n = 15−50) reveal the presence of several families of structural isomers: (1) *Ring Ia* (observed for n = 15−27 and 29) attributed to a monocyclic ring with a Nb^+ either inserted into or bound to the outside of the ring; (2) *Ring Ib* (n = 15, 17, 19, and possibly 21) attributed to a monocyclic ring with a Nb^+ sitting inside; (3) *Ring II* (n > 21) attributed to bicyclic rings where a Nb^+ links the rings together; (4) *Graphite* (n > 22) attributed to a roughly-planar metal-containing graphitic fragment; and (5) *Fullerene* (n > 27) including endohedral and networked isomers. As size increases, the relative abundance of the observed isomers progresses as monocyclic rings → bicyclic rings → graphitic sheets → metallofullerenes.

Comparison of these results to the results of similar studies for pure C_n^+ and LaC_n^+ shows that the nature of the metal atom can have a substantial effect on the observed isomers. The metal atom enhances the relative abundances of the graphitic sheet and fullerene isomers compared with the pure C_n^+ system. The metal also appears to inhibit formation of large NbC_n^+ monocyclic rings. Unlike the C_n^+ and LaC_n^+ analogues, the NbC_n^+ bicylic rings do not anneal into monocyclic rings. These differences are attributed to differences in the chemical properties of La^+ and Nb^+, and in particular the ability of Nb^+ to form more than two strong metal−carbon bonds.

Annealing studies show that NbC_n^+ bicyclic rings can be converted into graphitic sheets and metallofullerenes. This is believed to occur by a mechanism that is similar to that proposed to explain the formation of pure carbon fullerenes from C_n^+ rings. The graphitic sheet isomer forms for the smaller clusters where the strain energy associated with forming the fullerene is high.

Networked MC_{2n-1}^+ metallofullerenes probably form when the metal retains sufficient electron density to interact locally at the defect site on a fullerene with an odd number of carbon atoms. Metals with few valence electrons and low ionization energies, such as those found in group III (Sc, Y, and La) of the periodic table, are expected to lose electron density to the fullerene cage and maximize ionic interactions by forming endohedral metallofullerenes. On the other hand, metals in groups IV, V, and VI may form networked structures because they have 3, 4, and 5 valence electrons, respectively, and relatively high ionization energies.

Acknowledgment. We gratefully acknowledge the support of this work by the National Science Foundation (Grant No. CHE-9306900) and the Petroleum Research Fund (administered by the American Chemical Society). We are also grateful for many helpful conversations with Mr. Konstantin B. Shelimov.

JA9516470